



doi:10.1016/S0016-7037(03)00128-5

U/Th Systematics and ages of authigenic carbonates from Hydrate Ridge, Cascadia Margin: Records of fluid flow variations

B. M. A. TEICHERT,[†] A. EISENHAEUER,^{*,a} G. BOHRMANN,[†] A. HAASE-SCHRAMM, B. BOCK, and P. LINKE

GEOMAR, Forschungszentrum für marine Geowissenschaften, Wischhofstr. 1-3, 24148 Kiel, Germany

(Received July 5, 2002; accepted in revised form February 5, 2003)

Abstract—Uranium (U) concentrations and activity ratios ($\delta^{234}\text{U}$) of authigenic carbonates are sensitive recorders of different fluid compositions at submarine seeps of hydrocarbon-rich fluids (“cold seeps”) at Hydrate Ridge, off the coast of Oregon, USA. The low U concentrations (mean: $1.3 \pm 0.4 \mu\text{g/g}$) and high ^{234}U values (165–317‰) of gas hydrate carbonates reflect the influence of sedimentary pore water indicating that these carbonates were formed under reducing conditions below or at the seafloor. Their $^{230}\text{Th}/^{234}\text{U}$ ages span a time interval from 0.8 to 6.4 ka and cluster around 1.2 and 4.7 ka. In contrast, chemoherm carbonates precipitate from marine bottom water marked by relatively high U concentrations (mean: $5.2 \pm 0.8 \mu\text{g/g}$) and a mean $\delta^{234}\text{U}$ ratio of $166 \pm 3\%$. Their U isotopes reflect the $\delta^{234}\text{U}$ ratios of the bottom water being enriched in ^{234}U relative to normal seawater. Simple mass balance calculations based on U concentrations and their corresponding $\delta^{234}\text{U}$ ratios reveal a contribution of about 11% of sedimentary pore water to the bottom water. From the U pore water flux and the reconstructed U pore water concentration a mean flow rate of about $147 \pm 68 \text{ cm/a}$ can be estimated. $^{230}\text{Th}/^{234}\text{U}$ ages of chemoherm carbonates range from 7.3 to 267.6 ka. $^{230}\text{Th}/^{234}\text{U}$ ages of two chemoherms (Alvin and SE-Knoll chemoherm) correspond to time intervals of low sealevel stands in marine isotope stages (MIS) 2, 4, 5, 6, 7 and 8. This observation indicates that fluid flow at cold seep sites sensitively reflects pressure changes of the hydraulic head in the sediments. The $\delta^{18}\text{O}_{\text{PDB}}$ ratios of the chemoherm carbonates support the hypothesis of precipitation during glacial times. Deviations of the chemoherm $\delta^{18}\text{O}$ values from the marine $\delta^{18}\text{O}$ record can be interpreted as to reflect temporally and spatially varying bottom water and/or vent fluid temperatures during carbonate precipitation between 2.6 and 8.6°C. Copyright © 2003 Elsevier Science Ltd

1. INTRODUCTION

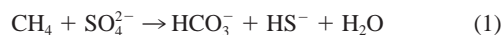
Submarine venting of hydrocarbon-rich, cold fluids into the seawater occurs in many different settings around the world (e.g., Kulm et al., 1986; Aharon et al., 1992; Polikarpov et al., 1992; Rendsbergen et al., 2002) and is thought to be due to the breakdown of gas hydrates deeper in the sedimentary column. Methane (CH_4), a main component of gas hydrates, is a strong greenhouse gas, which can potentially have a strong effect on global climate (e.g., Sloan et al., 1992; Hudson and Magoon, 2002). Therefore, it is critical to know whether venting from these cold seep sites is a continuous process or whether venting occurs discontinuously, and is controlled by external factors.

The subseafloor plumbing system of these cold seep sites is sometimes provided by faults. These faults tap at depth a fluid reservoir containing free gas (often methane) and reach up through the sediments to the seafloor (Moore et al., 1990). When the discharge area is situated within the gas hydrate stability field, seismic records often show a bottom simulating reflector (BSR). This reflector is interpreted to result from the contrast between hydrate-filled sediment above and a zone containing free gas below the BSR (Holbrook et al., 1996).

At the seafloor, the hydrocarbon emission sites are inhabited by a remarkable benthic chemosynthetic fauna of bivalves, tube worms and bacterial mats that derive their energy and nourish-

ment from oxidation of advecting reduced sulfur species and/or hydrocarbon compounds (Sibuet and Olu, 1998). In addition to the chemosynthetic communities, the venting sites are associated with authigenic carbonates that occur as extensive or sporadic seafloor pavements, concretions, chimney- or doughnut-like forms, and as steep and gently climbing carbonate mounds.

The carbonates are composed of aragonite, calcite or dolomite (Ferrel and Aharon, 1994; Bohrmann et al., 1998; Greinert et al., 2001). Different processes of carbonate formation can be distinguished. Their formation is triggered by the increase in alkalinity during anaerobic methane oxidation via sulfate reduction (AMO; see Eqn. 1).



The reaction is controlled by the upward flux of methane that reaches the sulfate zone and supports an interface of enhanced microbial activity. A consortium of methanogenic archaea and sulfate reducing bacteria that mediate the anaerobic oxidation of methane has recently been identified by Boetius et al. (2000). Carbonates precipitated in this environment will be formed close to the sediment surface and adjacent or even in gas hydrates (Bohrmann et al., 1998). These carbonates are known as gas hydrate carbonates and occur in two lithologies: as breccia composed of micrite-cemented monomict clasts and as pure aragonite precipitate (Bohrmann et al., 2002).

Another possible scenario of above-seafloor carbonate formation is characterized by vigorous methane flux from below through a network of fault zones. Carbonates will then be formed at the same place over a long period of time. Eventu-

* Author to whom correspondence should be addressed (aeisenhauer@geomar.de).

[†] Present address: Forschungszentrum Ozeanränder, Universität Bremen, Postfach 330440, 28334 Bremen, Germany.

ally, a carbonate mound can form above the fault system serving as an extended conduit into the ocean water (Aharon, 1994). Such carbonates are called chemoherm carbonates. The apparently most common lithologies of chemoherms are intraformational breccia and pure aragonite precipitates (Greiner et al., 2001). The surfaces of these carbonates are most probably inhabited by microbes generating a reducing micro-environment, which enables carbonate precipitation.

The emanation of hydrocarbons at any particular locality is likely to have a geologically short life span of unknown duration because of at least one of the following factors: (1) exhaustion of the hydrocarbon source, (2) changes in the tectonic activity causing the closure of old conduits and the opening of new ones, (3) clogging of the vent conduits due to carbonate precipitation and/or gas hydrate formation. The only substantial archive of the vent system remains in long-lasting carbonate build-ups (chemoherms), which are likely to contain a detailed chronology of the venting (Aharon et al., 1997).

In this study we present the first U/Th chronology of cold seep carbonates from the Hydrate Ridge area off the coast of Oregon, USA. Uranium concentrations and isotope ratios reveal the amount of pore water involved in the formation of gas hydrate- and chemoherm carbonates and allow an estimate of the pore water contribution to the bottom water. Furthermore, the $\delta^{18}\text{O}_{\text{PDB}}$ record of the chemoherm carbonates supports their formation during sealevel lowstands and allows the calculation of the seawater/fluid temperature.

2. GEOLOGY OF THE HYDRATE RIDGE AREA

The Cascadia subduction zone is located offshore of the northwestern United States (inset of Fig. 1). The Juan de Fuca plate is subducted to the north-east below the North American plate at a rate of about 40 mm/a (Goldfinger et al., 1997). Hydrate Ridge is the second ridge on the seaward-verging thrust sequence of the accretionary prism and has a north to south extension of about 25 km. A northern and southern summit can be distinguished (Fig. 1). The northern summit is about 200 m higher in elevation than the southern one.

The northern summit of Hydrate Ridge is dominated by the occurrence of massive carbonate boulders (“Boulder-Complex”) that cover the seafloor and several chemoherm build-ups. The Sonne and the Alvin chemoherm to the west and north-west of the summit are the most prominent chemoherms. The lithologies of both chemoherms are predominantly mudstones, mudclast breccia and intraformational breccia (Greiner et al., 2001). The mineralogy of the authigenic carbonates is aragonitic, calcitic and/or dolomitic. Both chemoherms have gently climbing flanks and heights of about 30 m. Gas hydrates were retrieved from the sediments of the northern Hydrate Ridge during ODP Leg 146 at Site 892A (Westbrook et al., 1994) and in tensional fractures between blocks of carbonates (Suess et al., 1999). Methane gas venting at the sea floor indicates that fluids from the zone of free gas beneath the BSR rise up rapidly through the gas hydrate stability zone (Tréhu et al., 1999; Torres et al., 2002).

At the southern summit of Hydrate Ridge, the seafloor is dominated by sediments with an undulating topography (Suess et al., 2001). The characteristic carbonates here are the gas hydrate carbonates (Bohrmann et al., 1998), which seem to be

more abundant on the southern than on the northern Hydrate Ridge. We have sampled pure aragonite gas hydrate carbonates down to a depth of about 40 cm below the seafloor. These carbonates are always associated with white or orange bacterial mats on the seafloor and gas hydrate underneath.

In 1999, a circa 50 m-high carbonate mound with steep, almost vertical flanks was discovered by the deep submergence vehicle (DSV) ALVIN and named “Pinnacle” (Torres et al., 1999; Fig. 1). It has a north to south extension of about 150 m and is located in a topographic depression. The lower slopes are covered with talus blocks several meters in diameter, which made sampling of in situ carbonates from the base of the chemoherm impossible. Characteristic for the mostly pure aragonitic chemoherm carbonates at the top is a very irregular shape and high porosity. The Pinnacle is a still active fluid pathway (Linke and Suess, 2001) indicated by emanating gas bubbles, bacterial mats and vesicomid clams like *Calyplogena* observed on the carbonate mound.

A similar chemoherm named “South-East Knoll” (Fig. 1) was discovered in 1999 during research cruise SO143 (Bohrmann et al., 2000) and further investigated in 2000 during research cruise SO148 (Linke and Suess, 2001). This prominent chemoherm has steep slopes and rises about 60 to 90 m from the seafloor. Fractures filled with bacterial mats and clams, as well as gas bubble discharges, indicate active fluid venting.

3. SAMPLE MATERIAL

We analyzed carbonate, sea- and pore water samples from four research cruises in 1996, 1999 and 2000 to Hydrate Ridge (Table 1). Sample 36-4-Z is from R/V SONNE cruise SO109 in 1996 (Herzig et al., 1997) and was retrieved from the Alvin chemoherm at the northern Hydrate Ridge. A calcitic carbonate (60-1-E; Fig. 2c) was sampled from the south-east flank of the northern Hydrate Ridge during the R/V SONNE cruise SO143 (TECFLUX I; Bohrmann et al., 2000). This vent area shows a complicated diapiric subseafloor structure. Most likely, the bone-shaped, elongated carbonates (up to 20 cm in diameter and 30 cm in length) represent cemented fluid pathways (“tube carbonate”). During the R/V SONNE cruise SO143 in 1999, gas hydrate carbonates (21-2-B, 55-5, 56-1-C, 56-1-H, 222-C; Fig. 2a) were collected with a video-guided grab sampler on the southern Hydrate Ridge. Sample 571-3-3 was retrieved from the southern Hydrate Ridge on the R/V SONNE cruise SO148 in 2000 (TECFLUX II; Linke and Suess, 2001). It is a very porous, poorly cemented rock, sticking half way out of the sediment cover. The high porosity, a sign for fluid and/or gas flow, is lined with pure, yellowish aragonite cement. During the R/V ATLANTIS cruise Leg AT3-35B (Torres et al., 1999) chemoherm carbonates from the top of the Pinnacle (3428-6, 3424-4 and 3429-3) were collected with DSV ALVIN’s manipulator arms. One sample (3424-4) is part of a boulder from the talus around the Pinnacle. During R/V SONNE cruise SO148 samples 570-1, 570-9 (Fig. 2b) and 571-2 were collected from the Pinnacle. All samples but one are from the top of the Pinnacle. Sample 565-7 is from the SE-Knoll and was sampled with the remotely operated vehicle (ROV) ROPOS’s manipulator arms (ROPOS: Remotely Operated Platform for Ocean Sciences). Sample 26 results from a collision of our

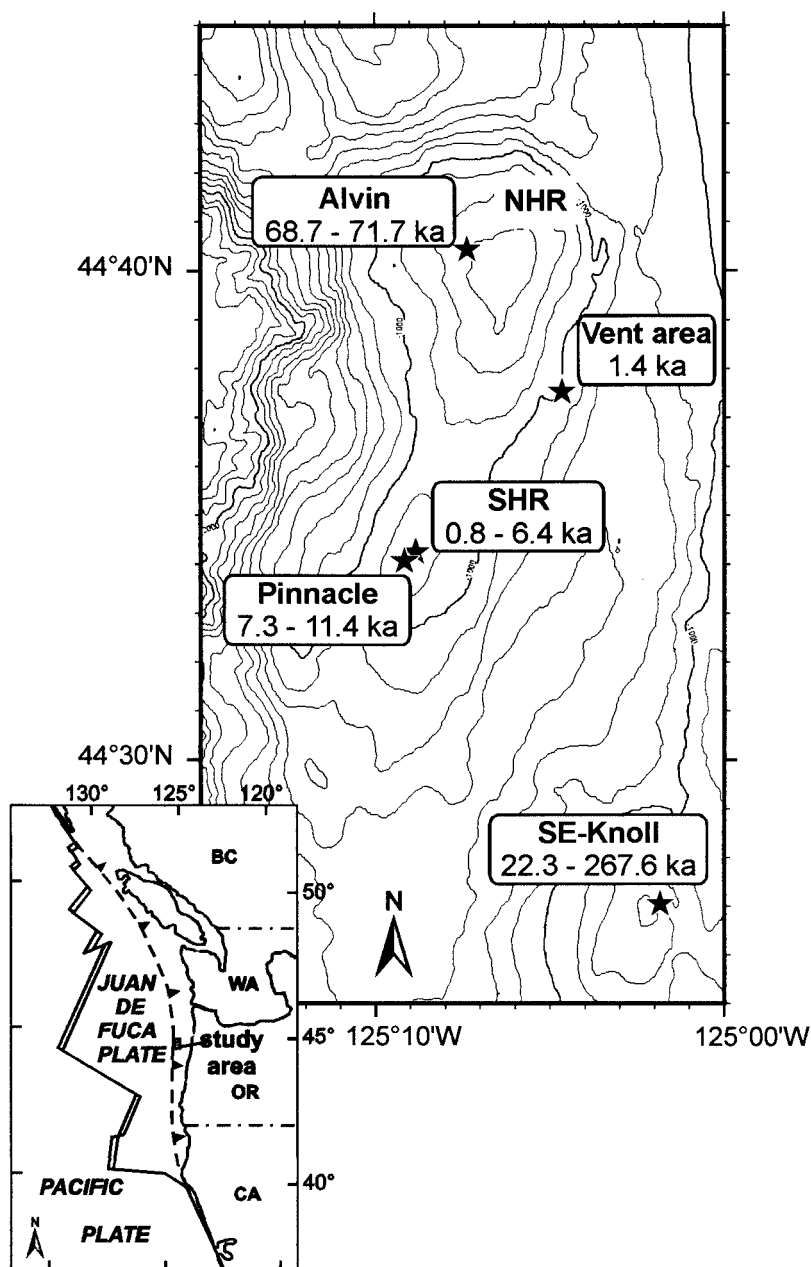


Fig. 1. Map shows the regional bathymetry of Hydrate Ridge. Filled stars mark sampling locations. Name of sampling area and calculated U/Th ages are given in the boxes (NHR: northern Hydrate Ridge, SHR: southern Hydrate Ridge). Inset shows plate tectonic setting of the Cascadia convergent margin (modified after Duncan and Kulm, 1989). Jagged, dashed line is the subduction zone.

OFOS (Ocean Floor Observation System) with the chemoherm SE-Knoll.

Bottom water was sampled by ROV ROPOS. Samples are from the location SO148/566-1 (bubbling vent location) and 571-1. All bottom water samples were taken about 5 to 10 m above seafloor.

Sediment pore water samples are from location SO143/55-2 (multicore) and 221-2 (gravity core) on the southern Hydrate Ridge. Both sites were active vent sites indicated by the occur-

rence of chemoautotrophic clams (*Calyptogena*), surficial bacterial mats and subseafloor gas hydrates.

4. SAMPLE PREPARATION AND ANALYTICAL METHODS

4.1. $^{230}\text{Th}/^{234}\text{U}$ Measurements

For U-series dating we chose 15 pure aragonite samples (>97 wt.% aragonite) and one sample composed of calcitic cemented sediment (high Mg-calcite with 11 mol.% MgCO_3 ; Table 1). The mineralogical

Table 1. Location of carbonate and water samples used in this study.

Sample	Cruise	Type	Location	Latitude °N	Longitude °W	Water depth (m)
21-2-B	SO143	GhC	SHR	44°34 212	125°08 810	788
55-5	SO143	GhC	SHR	44°34 210	125°08 830	787
56-1-C	SO143	GhC	SHR	44°34 220	125°08 798	787
56-1-H	SO143	GhC	SHR	44°34 220	125°08 798	787
222-C	SO143	GhC	SHR	44°34 238	125°08 843	772
571-3	SO148	GhC	SHR	44°34 216	125°08 810	766
3428-6-A	AT3-35b	CC	Pinnacle/SHR	44°34 092	125°09 046	774
3434-4-A	AT3-35b	CC	Pinnacle/SHR	44°34 104	125°09 170	812
3429-3-A	AT3-35b	CC	Pinnacle/SHR	44°34 100	125°09 170	772
570-1	SO148	CC	Pinnacle/SHR	44°34 094	125°09 141	762
571-2	SO148	CC	Pinnacle/SHR	44°34 107	125°09 172	776
570-9	SO148	CC	Pinnacle/SHR	44°34 088	125°09 180	762
26	SO148	CC	SE-Knoll	44°27 119	125°01 746	620
565-7	SO148	CC	SE-Knoll	44°26 989	125°01 966	616
36-4-Z	SO109	CC	Alvin/NHR	44°40 443	125°07 368	668
60-1-E	SO143	TC	vent area/NHR	44°37 560	125°04 670	924
571-1	SO148	bw	Pinnacle/SHR	44°34 120	125°09 167	769
566-1	SO148	bw	NHR	44°34 230	125°08 840	577
55-2 [#]	SO143	pw	SHR	44°34 230	125°08 840	788
221-2*	SO143	pw	SHR	44°34 211	125°08 811	785

composition was determined by X-ray diffraction (XRD). Standard XRD analyses allowed calculation of semiquantitative abundance of carbonate phases. All samples were cut and subsamples were taken using a microdrill. The weight of the analyzed samples varied from 0.17 to 1.12 g depending on the available material. The procedures for chemical separation and purification of U and Th, as well as the dating procedures, are close to those described by Chen et al. (1986) and Edwards et al. (1987), respectively. From the high Mg-calcite sample (60-1-E), we prepared three aliquots to obtain an U/Th-isochron. One aliquot was prepared for a whole rock analysis. From the other part, we separated the calcitic and the detrital aliquot by leaching the calcite one hour with 0.1 N suprapur acetic acid (Merck). Note, that all samples with $^{230}\text{Th}/^{232}\text{Th}$ activity ratios lower than 20 (almost all gas hydrate carbonates) have to be corrected for inherited ^{230}Th (Table 2). To correct for inherited ^{230}Th , we used the $^{230}\text{Th}/^{232}\text{Th}$ activity ratio of 1.92 of sample 60-1-Eb (detritus) as a representative for the local

sediments of Hydrate Ridge. To verify the corrected U/Th-ages (Table 2, column 10), we also calculated isochron ages. For the calculation of these isochron ages, we used the individual sample values and the value of sample 60-1-E as an initial value for all samples. Comparison of the ^{230}Th corrected U/Th ages with their corresponding isochron ages does not show any difference, which implies that the corrected U/Th-ages can be considered reliable.

For pore water analyses, cores were capped directly after retrieval and immediately transferred to the cold room. Squeezing was performed immediately after recovery at 4°C under argon gas atmosphere at about 3 atm. The bulk solution was filtered into acid cleaned bottles. The two pore water samples were acidified and ultrasonically treated before chemical separation.

After retrieval of the bottom water samples from ROV ROPOS's Niskin bottles (SO148), the bulk solution was filtered, acidified, and transferred to previously cleaned polyethylene bottles.

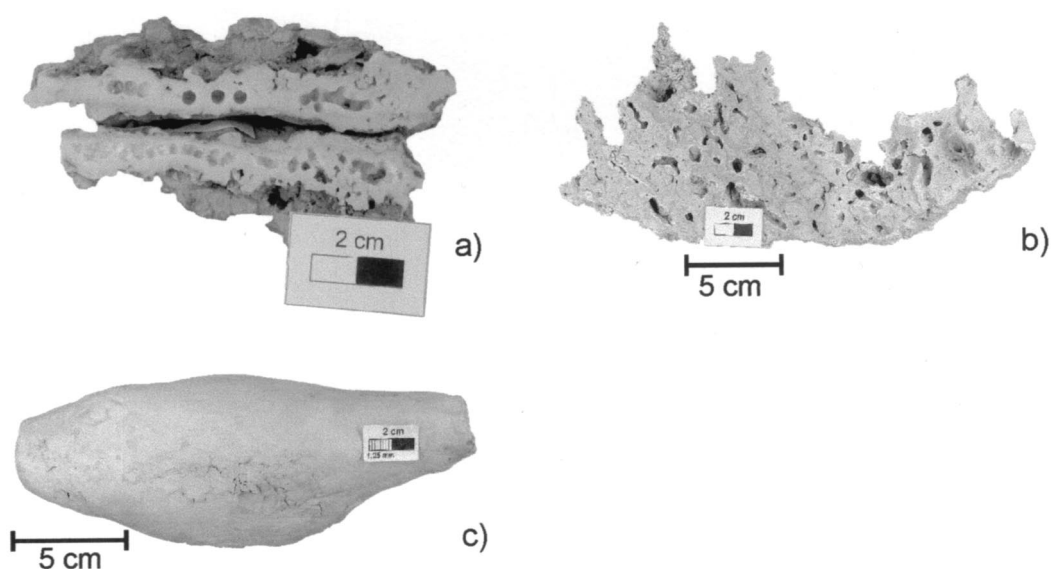


Fig. 2. Different types of authigenic carbonates: (a) Pure, aragonitic gas hydrate carbonate (sample 21-2-B). (b) Pure, aragonitic chemoherm carbonate with very irregular shape and high porosity (sample 570-9). (c) Calcitic tube carbonate (sample 60-1).

Table 2. U and Th isotopic compositions of authigenic carbonates, bottom- and pore water and $^{230}\text{Th}/^{234}\text{U}$ ages of authigenic carbonates.

Sample	Location	^{238}U ($\mu\text{g/g}$)	^{230}Th (pg/g)	$^{230}\text{Th}/^{232}\text{Th}$ activity ratio	$\delta^{234}\text{U}_{(0)}$ (%)	$\delta^{234}\text{U}_{(T)}$ (%)	$^{230}\text{Th}/^{234}\text{U}$ activity ratio	Age (a)	Age (a) Th corr.
21-2-B-1	SHR	1.1406 ± 0.0009	0.39 ± 0.03	5.5 ± 0.4	214 ± 5	215 ± 5	0.017 ± 0.001	1,900 ± 300	1,300 ± 400
21-2-B-2	SHR	1.1561 ± 0.0005	0.341 ± 0.005	7.6 ± 0.1	166 ± 4	167 ± 4	0.0155 ± 0.0002	1,700 ± 100	1,300 ± 200
55-5-3	SHR	1.377 ± 0.001	0.63 ± 0.02	2.8 ± 0.1	164 ± 4	164 ± 4	0.0240 ± 0.0006	2,600 ± 100	800 ± 900
56-1-C-2	SHR	1.4907 ± 0.0008	1.01 ± 0.03	89.8 ± 3.2	173 ± 4	175 ± 4	0.032 ± 0.001	3,500 ± 300	3,400 ± 300
56-1-C-1	SHR	0.3451 ± 0.0004	0.14 ± 0.02	18.3 ± 0.7	315 ± 5	317 ± 5	0.019 ± 0.003	2,000 ± 700	1,800 ± 700
56-1-C-5	SHR	1.812 ± 0.001	1.53 ± 0.03	14.7 ± 0.3	178 ± 4	180 ± 4	0.044 ± 0.001	4,900 ± 200	4,300 ± 400
56-1-H-1	SHR	1.885 ± 0.001	2.01 ± 0.03	8.1 ± 0.1	187 ± 4	189 ± 4	0.0550 ± 0.0008	6,200 ± 200	4,800 ± 700
56-1-H-2	SHR	1.600 ± 0.003	2.16 ± 0.05	9.7 ± 0.2	175 ± 8	179 ± 8	0.070 ± 0.002	7,800 ± 400	6,400 ± 800
222-C-1	SHR	0.8159 ± 0.0005	0.300 ± 0.008	6.0 ± 0.2	207 ± 2	208 ± 2	0.0186 ± 0.0005	2,000 ± 100	1,400 ± 300
571-3-3	SHR	2.581 ± 0.001	0.59 ± 0.03	6.2 ± 0.3	170 ± 3	171 ± 3	0.0120 ± 0.0005	1,300 ± 100	800 ± 300
3428-6-A-1	Pinnacle/SHR	4.569 ± 0.002	8.2 ± 0.2	1076 ± 31	153 ± 3	158 ± 3	0.095 ± 0.003	10,800 ± 600	10,900 ± 600
3424-4-A-2	Pinnacle/SHR	4.439 ± 0.003	5.48 ± 0.06	1009 ± 11	156 ± 6	159 ± 6	0.065 ± 0.001	7,300 ± 200	7,300 ± 200
3429-3-A-2	Pinnacle/SHR	6.806 ± 0.003	10.4 ± 0.2	398 ± 6	155 ± 4	159 ± 4	0.081 ± 0.001	9,100 ± 300	9,200 ± 300
3429-3-A-8a	Pinnacle/SHR	6.396 ± 0.005	9 ± 1	924 ± 108	155 ± 8	159 ± 8	0.078 ± 0.009	8,900 ± 2,000	8,800 ± 2,000
3429-3-A-8b	Pinnacle/SHR	6.396 ± 0.005	11.9 ± 0.5	1338 ± 61	158 ± 6	163 ± 6	0.099 ± 0.004	11,400 ± 1,000	11,400 ± 1,000
570-1-3	Pinnacle/SHR	5.442 ± 0.002	7.73 ± 0.04	1025 ± 5	149 ± 3	153 ± 3	0.0755 ± 0.0004	8,500 ± 100	8,500 ± 100
571-2-1	Pinnacle/SHR	4.529 ± 0.003	7.3 ± 0.1	690 ± 10	167 ± 5	171 ± 5	0.085 ± 0.001	9,600 ± 300	9,700 ± 300
571-2-2	Pinnacle/SHR	5.005 ± 0.002	8.0 ± 0.5	1777 ± 111	149 ± 2	153 ± 2	0.085 ± 0.005	9,700 ± 1,200	9,800 ± 1,200
570-9-5	Pinnacle/SHR	5.088 ± 0.002	9.06 ± 0.07	1794 ± 14	158 ± 2	160 ± 2	0.095 ± 0.001	11,000 ± 200	10,900 ± 200
26	SE-Knoll	2.389 ± 0.003	38.52 ± 0.08	4905 ± 25	60 ± 6	127 ± 6	0.930 ± 0.002	267,700 ± 5,500	267,600 ± 5,500
26-1	SE-Knoll	3.191 ± 0.001	45.7 ± 0.3	14065 ± 83	77 ± 3	128 ± 3	0.817 ± 0.004	177,300 ± 4,200	177,700 ± 4,200
26-3	SE-Knoll	8.416 ± 0.004	132.2 ± 0.4	15595 ± 59	82 ± 3	153 ± 3	0.887 ± 0.003	221,500 ± 4,500	221,700 ± 4,500
565-7-7	SE-Knoll	4.412 ± 0.001	15.8 ± 0.2	633 ± 9	155 ± 2	168 ± 2	0.189 ± 0.003	22,300 ± 700	22,300 ± 700
36-4-Z-1	Alvin/NHR	3.606 ± 0.002	31.9 ± 0.2	1023 ± 8	139 ± 4	168 ± 4	0.474 ± 0.003	68,900 ± 1,400	68,700 ± 1,400
36-4-Z-2	Alvin/NHR	6.684 ± 0.002	61.1 ± 0.2	343.8 ± 1.4	138 ± 2	169 ± 2	0.490 ± 0.002	72,000 ± 600	71,700 ± 600
60-1-Ea, total	vent area/NHR	1.1300 ± 0.0004	16.40 ± 0.05	1.844 ± 0.006	63 ± 2		0.828 ± 0.003		
60-1-Eb, calcite	vent area/NHR	0.6377 ± 0.0005	0.27 ± 0.01	6.7 ± 0.3	153 ± 4	152 ± 4	0.0179 ± 0.0008	2,000 ± 200	1,400 ± 300
60-1-Eb, detritus	vent area/NHR	1.0497 ± 0.0004	17.2 ± 0.6	1.92 ± 0.07	37 ± 2		0.95 ± 0.03		
<i>Bottom water</i>		(ng/g)							
571-1a	Pinnacle/SHR	2.882 ± 0.004			168 ± 7				
571-1b	Pinnacle/SHR	3.128 ± 0.005			163 ± 9				
566-1	NHR	2.856 ± 0.003			166 ± 7				
<i>Pore water</i>									
55-2-C	SHR	6.291 ± 0.006			153 ± 7				
221-2a	SHR	6.056 ± 0.005			352 ± 9				
221-2b	SHR	5.81 ± 0.01			361 ± 21				

Uranium- and Th isotope dilution measurements were performed with a $^{233}\text{U}/^{236}\text{U}$ double spike and a ^{229}Th single spike by thermal ionisation mass spectrometry (TIMS) on a Finnigan MAT 262 RPQ⁺ at the GEOMAR Forschungszentrum, Kiel, Germany. Thirty-one measurements of New Brunswick Laboratories Certified Reference Material 112a (NBL-112a, formerly NBS SRM 960 and CRM-145) gave a mean $^{234}\text{U}/^{238}\text{U}$ atomic ratio of $5.31 \pm 0.04 \cdot 10^{-5}$ (2 s.d.: two standard deviations) corresponding to a $\delta^{234}\text{U}_{(0)}$ value of $-33 \pm 7\%$ ($\delta^{234}\text{U}_{(0)} = ((^{234}\text{U}/^{238}\text{U})_{\text{activity ratio}} - 1) \cdot 1000$) based on the recently new defined decay constant of ^{234}U (Cheng et al., 2000b). Our $\delta^{234}\text{U}_{(0)}$ mean value of NBL-112a tends to be about 3 to 4‰ higher than that of previous measurements, but is still in statistical accordance with the earlier reported $\delta^{234}\text{U}_{(0)}$ values of Cheng et al. (2000b): $-37 \pm 8\%$ (2 s.d.), Eisenhauer et al. (1996): $-36 \pm 4\%$ (2 s.d.) and Edwards et al. (1993): $-37 \pm 3\%$ (2 s.d.). Note, that the Eisenhauer et al. (1996) and Edwards et al. (1993) values were recalculated with the new decay constant for ^{234}U from Cheng et al. (2000b).

4.2. $\delta^{18}\text{O}$ Measurements

Carbonate samples for determination of oxygen stable isotopes were obtained by using a hand-held microdrill. Carbonate powders were reacted with 100% phosphoric acid (density >1.9; Wachter and Hayes, 1985) at 75°C in an online carbonate preparation line (Carbo-Kiel-single sample acid bath) connected to a Finnigan Mat 252 mass spectrometer (Geologisches Institut der Universität Erlangen, Germany). All values are reported in permil (‰) relative to V-PDB (Peedee

Belemnite) by assigning a $\delta^{18}\text{O}$ value of -2.20% PDB to NBS 19. Results are expressed in the usual δ -notation relative to the PDB-standard. Reproducibility was verified by replicate analyses of laboratory standards and is better than about 0.02‰ (1 σ) for $\delta^{18}\text{O}$.

4.3. Determination of Ca Concentrations

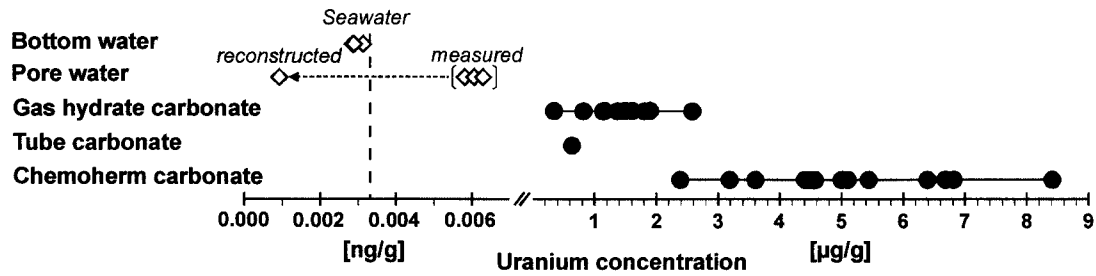
Ca concentrations of a pore water sample and authigenic carbonates were determined by ICP-AES (JY 170 Ultratrace) at GEOMAR Forschungszentrum, Kiel, Germany. For the carbonates, repeated measurements (n=6) of a Ca-standard (Spex) gave a reproducibility of 13 $\mu\text{g/g}$ (2 s.d.), which corresponds to a statistical uncertainty of about 5%. Accuracy was verified by repeated measurements of the IAPSO seawater standard.

5. RESULTS AND DISCUSSION

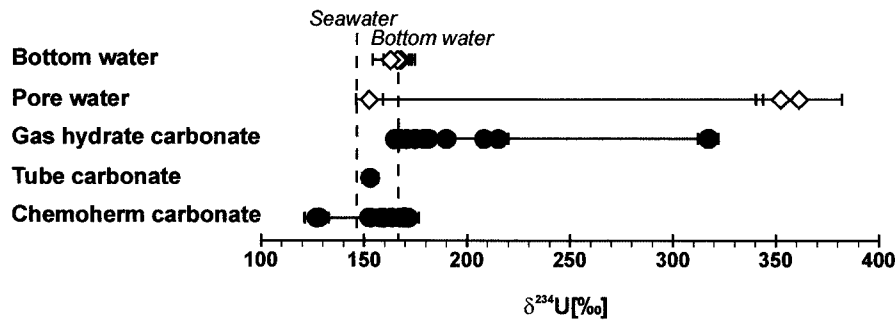
5.1. U Concentrations and $\delta^{234}\text{U}$ in Bottom Water, Pore Water and Authigenic Carbonates

All U and Th results are given in Table 2 and are graphically displayed in Figure 3a–c. The U concentrations of our bottom water samples (U_{bw} ; average: 3.0 ± 0.2 ng/g) are about 4 to 12% lower than the expected uranium seawater concentration (U_{sw}) of 3.261 ± 0.007 ng/g for the Pacific Ocean (Chen et al.,

a)



b)



c)

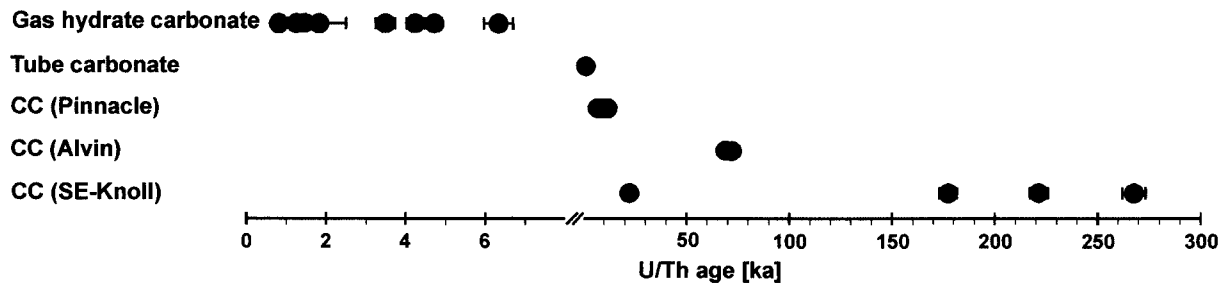


Fig. 3. (a) Uranium concentrations of chemoherm-, tube- and gas hydrate carbonates, pore- and bottom water are plotted together. Note the break in scale and changing units. Measured U_{pw} are in brackets. Arrow points to the reconstructed U_{pw} . Dashed vertical line gives the seawater U concentration of Chen et al. (1986). (b) $\delta^{234}U$ ratios of chemoherm-, tube- and gas hydrate carbonates, pore- and bottom water are plotted together. Dashed vertical lines mark the literature $\delta^{234}U$ value of modern “seawater” (Cheng et al., 2000a) and measured “bottom water” (mean value) at Hydrate Ridge (this work). (c) $^{230}Th/^{234}U$ ages of chemoherm-, tube- and gas hydrate carbonates. Note the break in scale.

1986) whereas uranium concentrations in the pore water (U_{pw}) are about a factor of 2 higher than bottom water (Fig. 3a). The average $\delta^{234}U$ value of the bottom water samples of $166 \pm 3\%$ (2 s.d.) is higher than the presently accepted mean value for modern seawater of $145.8 \pm 1.7\%$ (Cheng et al., 2000a; Fig. 3b). The $\delta^{234}U$ values of all pore water samples are generally higher than bottom water and show a large variation in their $\delta^{234}U$ ratios from 153 to 361‰ (Fig. 3b).

The average U concentration of the gas hydrate carbonates (U_{GhC}) and the calcite fraction of the tube carbonate (average U_{GhC} : $1.4 \pm 0.4 \mu\text{g/g}$) is almost a factor of 4 lower than the

average chemoherm carbonate U concentration (U_{CC} ; average U_{CC} : $5.2 \pm 0.8 \mu\text{g/g}$; Fig. 3a). The $\delta^{234}U$ ratios of the chemoherm carbonates cluster closely around an average value of about $161 \pm 4\%$ (except for samples 26 and 26-1) being close to the mean value of our measured bottom water ($166 \pm 3\%$). In contrast, the $\delta^{234}U$ activity ratios of the gas hydrate carbonates show a large variation, similar to that of the sediment pore water, from about 165 to 317‰. Such variations occur even within the aragonitic layer of a single carbonate sample (e.g., sample 21-2-B).

The U concentration of suboxic to anoxic pore water is

expected to be lower than seawater because U is highly soluble under oxic conditions but highly insoluble under reducing conditions (cf. Barnes and Cochran, 1988). Consequently, the U_{GhC} (mean: $1.4 \pm 0.4 \mu\text{g/g}$) precipitated from anoxic pore water is expected to be lower than the U_{CC} (mean: $5.2 \pm 0.8 \mu\text{g/g}$) precipitated from the bottom water (Table 2, Fig. 3a). In contrast to the expected low U concentrations in the pore water, our pore water samples are enriched in U (mean: $6.1 \pm 0.3 \text{ ng/g}$). They are even enriched relative to the U concentrations of our bottom water samples (mean: $3.0 \pm 0.2 \text{ ng/g}$; Fig. 3a). Therefore, we propose that these values do not reflect the original U_{pw} ; rather, they reflect the reoxidizing and leaching of U from the adjacent sediment during pore water sampling procedures onboard the research vessel. Henderson et al. (1999) have documented enrichment of U in pore water squeezed under air. Thus, the measured U concentrations are not considered to be representative of pore water and are neglected in the following discussion.

To reconstruct U_{pw} , we can use two different approaches: (1) a simple binary mixing calculation, and (2) using the calculated partition coefficient (K_d) for the U/Ca ratio in aragonite. Following approach (1) we may calculate from the average $\delta^{234}\text{U}$ ratio of pore water ($357 \pm 6\%$), bottom water ($166 \pm 3\%$) and normal seawater ($145.8 \pm 1.7\%$; Cheng et al., 2000a) that the bottom water consists of about 90% normal seawater and about 10% pore water (see Appendix 1). U_{pw} can be estimated to be of the order of about $0.1 \pm 0.2 \text{ ng/g}$ ($\delta^{234}\text{U}_{pw} = 357 \pm 6\%$, $\delta^{234}\text{U}_{bw} = 166 \pm 3\%$). However, this value has a large statistical uncertainty, because of the small contribution of U_{pw} to U_{bw} by propagation of errors. Therefore, we also use an alternative way to estimate U_{pw} .

Our second approach (2) is to calculate a partition coefficient (K_d) with:

$$K_d = \left(\frac{U}{Ca} \right)_{CC} / \left(\frac{U}{Ca} \right)_{sw} \quad (2)$$

for U in aragonite of about 1.83 at 4.7°C (with mean $U_{CC} = 5.16 \mu\text{g/g}$ (see Table 2); mean $Ca_{CC} = 356000 \pm 5000 \mu\text{g/g}$ (2 s.d., $n=11$); $U_{sw} = 3.261 \text{ ng/g}$, Chen et al., 1986; average seawater (IAPSO) $Ca_{sw} = 412 \mu\text{g/g}$).

With the K_d of 1.83, we can then calculate U_{pw} to be about $0.24 \pm 0.06 \text{ ng/g}$ with a measured Ca concentration in the pore water (Ca_{pw}) of $110 \mu\text{g/g}$ (gravity core 221-2, 1.15 m depth) and the mean values of U and Ca concentrations in the gas hydrate carbonates (mean $U_{GhC} = 1.4 \mu\text{g/g}$ (see Table 2); mean $Ca_{GhC} = 361 \pm 7 \mu\text{g/g}$ (2 s.d., $n=12$)). The calculated value may be considered as a reliable approximation of the true U_{pw} , although we are aware of the fact that the U concentration in carbonate depends on many other factors apart from the U concentration of the precipitating fluid. Mineralogy is obviously important, as is the morphology of the mineral. Other factors such as temperature are also known to play a role in some carbonates (e.g., Shen and Dunbar, 1995). Although our calculated value for U_{pw} certainly has a considerable degree of uncertainty, it is most likely more reliable than those based upon measurements that contain systematic errors due to reoxidizing of pore water during the sampling procedure. In addition, from a statistical point of view our K_d approach (2) provides a much more precise constrain on the original U_{pw}

than the binary mixing approach (1). Previously reported values of U concentrations in reduced pore waters are in the same range of about 0.93 to 0.07 ng/g (Henderson et al., 1999).

5.2. Quantification of the Exchange of Uranium across the Sediment Seawater Interface above Cold Seep Areas

5.2.1. Mixing of pore water uranium with seawater uranium

As a consequence of the α -recoil effect, the $\delta^{234}\text{U}$ ratio of sedimentary pore water tends to be higher than the $\delta^{234}\text{U}$ ratio of seawater (Kigoshi, 1971) resulting in an increase of the $\delta^{234}\text{U}$ ratio in gas hydrate carbonates (Table 2, Fig. 3b). Our observations also show that the average $\delta^{234}\text{U}$ value of the chemoherm carbonates ($161 \pm 4\%$) as well as for the bottom water samples ($166 \pm 3\%$) is significantly higher than the expected seawater value (145.8% ; Cheng et al., 2000a). The latter observation may reflect a net flux of ^{234}U enriched pore water from the sediment to the seawater above the cold seep area. This water mass above the cold seep area is then enriched in ^{234}U and therefore has a different isotopic signature than normal seawater. Using a simple box model we are able to estimate the contribution of the pore water U flux (F_{pw}) relative to U seawater flux (F_{sw}) (see Appendix 2).

From the average $\delta^{234}\text{U}$ values of the seawater ($\delta^{234}\text{U}_{sw} = 145.8\%$; Cheng et al., 2000a), the bottom water ($\delta^{234}\text{U}_{bw} = 166\%$) and the deep pore water ($\delta^{234}\text{U}_{pw} = 357\%$) we are able to calculate a ratio of the U pore water flux to the U seawater flux of the order of 0.11. The latter value indicates that about 11% of the U present in the bottom water is supplied from the sedimentary pore water. If we calculate the pore water contribution for the chemoherm carbonates, we obtain a value of about 8% (with $\delta^{234}\text{U}_{CC} = 161\%$). Note that both values are in good agreement, although the 11% pore water contribution to the bottom water is a recent, single measurement value, while the 8% for the chemoherm carbonate is a mean value over time. In addition, our values are also consistent with earlier estimates based on the major ion composition of ambient bottom water where vent fluids contribute about 4 to 12% to the bottom water (Suess et al., 1999).

5.2.2. Estimation of uranium fluxes out of cold seep sediments

The value for the U pore water flux (F_{pw}) can be quantified from previously determined U seawater fluxes (F_{sw}) into organic rich sediments, which are summarized in Ivanovich and Harmon (1992). Values for F_{sw} vary in between $100 \text{ ng}/(\text{cm}^2 \cdot \text{a})$ (Barnes and Cochran, 1990) in the Black Sea to about $770 \text{ ng}/(\text{cm}^2 \cdot \text{a})$ for the Baltic Sea (Nikolayev et al., 1966). A mean value for the available U fluxes into organic rich sediments corresponds to about $321 \pm 148 \text{ ng}/(\text{cm}^2 \cdot \text{a})$ (2σ , $n=10$). Note, that U fluxes into organic rich sediments are on average a factor of 8 higher (Ivanovich and Harmon, 1992) than those into oxic and suboxic sediments. If we take the calculated value for the contribution of sedimentary pore water into account (11%), we can calculate a mean value of $35 \pm 16 \text{ ng}/(\text{cm}^2 \cdot \text{a})$ with a minimum and maximum value for F_{pw} in the order of about $11 \text{ ng}/(\text{cm}^2 \cdot \text{a})$ and $85 \text{ ng}/(\text{cm}^2 \cdot \text{a})$, respectively.

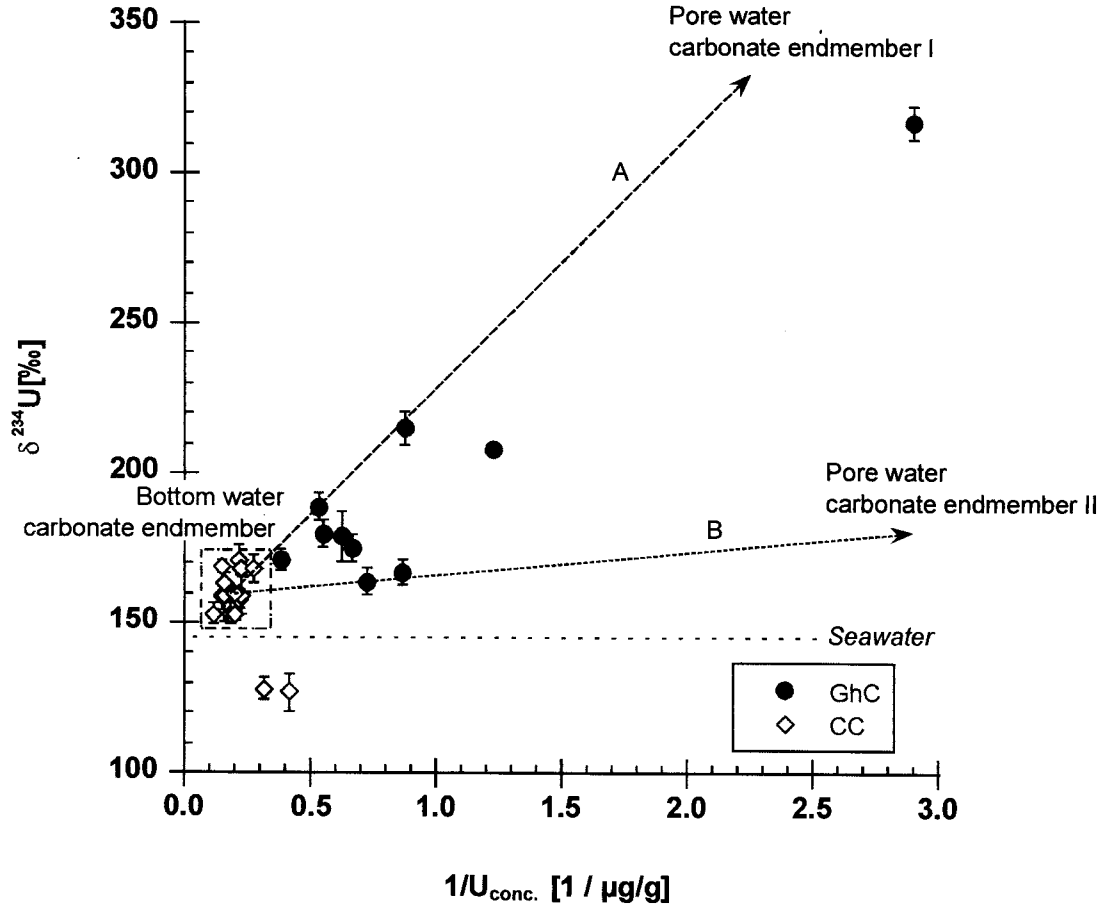


Fig. 4. Inverse U concentrations of authigenic carbonates are plotted as a function of their corresponding $\delta^{234}\text{U}_{(T)}$. Chemoherm carbonates (CC) cluster closely in a square, marked by a dashed line. Dashed horizontal line marks the present day $\delta^{234}\text{U}$ ratio (Cheng et al., 2000a). Line A and B represent mixing lines with a well-defined bottom water carbonate endmember represented by the chemoherm carbonates and a less well-defined pore water carbonate endmember represented by the gas hydrate carbonates (GhC).

5.2.3. Constraints on average advection rates

To constrain advection rates (v) related to cold seep environments, values of 46 cm/a to 353 cm/a (mean: 147 ± 68 cm/a) can be calculated with:

$$v = \frac{F_{pw}}{U_{pw}} \quad (3)$$

from the F_{pw} values and our reconstructed U pore water concentration (U_{pw}) of about 0.24 ng/g.

Our F_{pw} values can hardly be verified because direct measurements of U fluxes are difficult to perform. However, the calculated flow rate can be compared with other independent estimates of flow rates at Hydrate Ridge. At the northern and southern Hydrate Ridge direct measurements of in- and outflow of fluids revealed a flow rate of about 10 cm/a at clam sites to 1000 cm/a at areas covered with microbial mats indicative of extensive outflow of methane-rich fluids. At the southern Hydrate Ridge tide-controlled flow rates in the order of mm/a to cm/a have been observed (Tryon and Brown, 2001). These flow

rates are in general agreement with the results presented in this study.

5.2.4. Constraints on the origin of the uranium in gas hydrate carbonates

Evidence that gas hydrate carbonates are formed by the contribution of pore- and bottom water penetrating into the sediments comes from the observation that gas hydrate carbonates seem to form mixing lines with two or even more endmembers (Fig. 4). The average U concentrations and $\delta^{234}\text{U}$ ratios of the chemoherm carbonates represent one well-defined “bottom water carbonate endmember” solely precipitated from ocean bottom water. The “pore water carbonate endmember” (I and II) is a carbonate solely formed from sedimentary pore water. However, the “pore water carbonate endmember” is not well-defined because U concentrations and $\delta^{234}\text{U}$ may vary to a large extent depending on the rate and direction of fluid flow, redox conditions and other chemical factors. Thus, the slope of the mixing lines depends on the composition of the fluid, which may contain varying amounts of pore- and bottom water (Fig.

Table 3. Measured $\delta^{18}\text{O}_{\text{PDB}}$ of chemoherm carbonate samples, $\Delta\delta^{18}\text{O}_{\text{PDB}}$ from Karner et al. (2002), past $\delta^{18}\text{O}_{\text{SMOW}}$ seawater values, fractionation factor $\alpha_{\text{aragonite-seawater}}$, reconstructed past seawater/fluid temperature and marine isotopic stages (MIS) in chronological order.

Sample	Location	Age [ka]	$\delta^{18}\text{O}_{\text{PDB}}$ of sample [‰]	$\delta^{18}\text{O}_{\text{SMOW}}$ of sample [‰]	$\Delta\delta^{18}\text{O}_{\text{PDB}}$ Karner et al. (2002) [‰]	$\delta^{18}\text{O}_{\text{SMOW}}$ of seawater [‰]	$\alpha_{\text{arag.-sw}}$	T of fluid/SW [°C]	MIS
3424-4-A-2	Pinnacle	7.3 ± 0.2	3.95 ± 0.03	34.93	-0.64	-0.02	1.03496	2.6	I
570-1-3	Pinnacle	8.5 ± 0.1	4.02 ± 0.03	35.00	-0.58	0.05	1.03495	2.6	I
3429-3-A-2	Pinnacle	9.2 ± 0.3	3.78 ± 0.03	34.76	-0.52	0.10	1.03465	3.9	I
571-2-1	Pinnacle	9.7 ± 0.3	4.12 ± 0.01	35.10	-0.48	0.15	1.03495	2.7	I
571-2-2	Pinnacle	9.8 ± 1.2	3.95 ± 0.04	34.93	-0.47	0.16	1.03477	3.4	I
3429-3-A-8	Pinnacle	10.1 ± 1.5	3.78 ± 0.03	34.76	-0.45	0.18	1.03458	4.2	I
3428-6-A-1	Pinnacle	10.9 ± 0.6	4.00 ± 0.04	34.98	-0.37	0.26	1.03471	3.6	I
570-9-5	Pinnacle	10.9 ± 0.2	4.04 ± 0.03	35.02	-0.38	0.25	1.03476	3.4	I
565-7-7	SE-Knoll	22.3 ± 0.7	4.08 ± 0.03	35.07	0.46	1.11	1.03392	6.8	II
36-4-Z-1	Alvin	68.7 ± 1.4	3.45 ± 0.02	34.42	0.24	0.89	1.03350	8.6	IV
36-4-Z-2	Alvin	71.7 ± 0.6	3.86 ± 0.02	34.84	0.17	0.82	1.03400	6.5	V
26-1	SE-Knoll	177.7 ± 4.2	4.34 ± 0.03	35.34	0.34	0.99	1.03431	5.2	VI
26-3	SE-Knoll	221.7 ± 4.5	3.99 ± 0.04	34.97	-0.35	0.28	1.03468	3.7	VII
26	SE-Knoll	267.6 ± 5.5	4.17 ± 0.03	35.16	0.34	0.99	1.03414	5.9	VIII

4). Following our simplified approach, we propose for mixing line “A” that “pore water carbonate endmember I” represents a carbonate precipitated from anoxic sedimentary pore water highly enriched in ^{234}U but depleted in U. Whereas for mixing line “B,” “pore water carbonate endmember II” corresponds to a carbonate precipitated from a fluid with relatively low $\delta^{234}\text{U}$ ratios but high U concentrations.

5.3. $^{230}\text{Th}/^{234}\text{U}$ Ages of Authigenic Carbonates from Hydrate Ridge

5.3.1. $^{230}\text{Th}/^{234}\text{U}$ ages of gas hydrate carbonates

The gas hydrate carbonate samples from five different stations at the southern Hydrate Ridge show U/Th ages in between 0.8 and 6.4 ka (Table 2, Figs. 1 and 3c). It seems that there are two time intervals of enhanced carbonate precipitation. One relatively recent period with a mean age around 1.2 ± 0.3 ka (21-2-B, 55-5, 56-1-C-1, 222-C, 571-3) and an older period around 4.7 ± 1.2 ka (56-1-C-2, 56-1-C-5, 56-1-H). Gas hydrate carbonate precipitation is closely linked to the supply of methane-rich fluids. Hence, the environmental conditions during these two time intervals must have been favorable for enhanced methane fluxes through the sediment. We speculate that earthquakes or other tectonic movements opened new and enlarged old conduits for the supply of methane-rich fluids at Hydrate Ridge. In addition, second order sealevel variations introduced by vertical neotectonic movement along the west coast of the USA may also have opened new conduits through the sediment to the ocean bottom water (Pirazzoli, 1991).

Our observation that U/Th ages cluster in certain periods indicates that carbonate precipitation is not continuous but rather occurs in distinct intervals.

5.3.2. $^{230}\text{Th}/^{234}\text{U}$ ages of chemoherm carbonates

The chemoherm carbonate samples from the Alvin, Pinnacle and SE-Knoll chemoherm are older than the gas hydrate carbonates. Their ages vary between 7.3 and 267.6 ka (Table 2 and Fig. 3c). The youngest chemoherm is the Pinnacle with ages

ranging from 7.3 to 11.4 ka. The Alvin chemoherm has a minimum age of 68.7 to 71.7 ka. The samples from the SE-Knoll show the oldest ages ranging from 22.3 up to 267.6 ka.

Except for the samples from the Pinnacle, the ages of all the other chemoherm carbonates correspond to time intervals of low sealevel in marine isotope stages (MIS: 2, 4, 5, 6, 7, 8; Table 3). Given that this coincidence is statistically significant, our observation appears to imply that the growth of the chemoherms is a discontinuous process with relatively high rates of carbonate precipitation, probably induced by enhanced methane degassing during glacial periods, and lower or even negligible rates of carbonate precipitation during interglacial periods related to decreased methane degassing. The relationship of carbonate precipitation, glacial periods and sea level lowstands, as well as the exception of the Pinnacle samples, will be discussed in the section below.

5.4. $\delta^{18}\text{O}$ Variations and Reconstruction of Seawater Temperature during Chemoherm Precipitation

Our observation that the chemoherm carbonates are predominantly precipitated during glacial periods is supported by their corresponding $\delta^{18}\text{O}_{\text{PDB}}$ ratios (Table 3). The measured $\delta^{18}\text{O}_{\text{PDB}}$ ratios of the chemoherm carbonates are up to 0.9‰ enriched in ^{18}O relative to their expected modern isotope equilibrium value of $\delta^{18}\text{O}_{\text{PDB}} = 3.47\text{‰}$ for a modern bottom water temperature of about 4.7°C and relative to a $\delta^{18}\text{O}_{\text{SMOW}}$ ratio of 0‰ (corresponding -29.94 (PDB)) for modern seawater ($\delta^{18}\text{O}_{\text{PDB}} = 0.97006 \cdot \delta^{18}\text{O}_{\text{SMOW}} - 29.94$; Friedman and O’Neil, 1977). The latter observation of heavier values than the expected modern equilibrium value may correspond to the observation that during glacial periods the $\delta^{18}\text{O}_{\text{SMOW}}$ of seawater tends to be heavier than the present value due to the amount of seawater stored in the continental ice shields (Schrag et al., 1996). The exact value for the different glacial periods is still under discussion although Duplessy et al. (2002) give a value of about 1.05‰ as a good estimate for variation of the $\delta^{18}\text{O}$ of deep-ocean water between the Last Glacial Maximum (LGM) and the Holocene. However, this 1.05‰ variation does

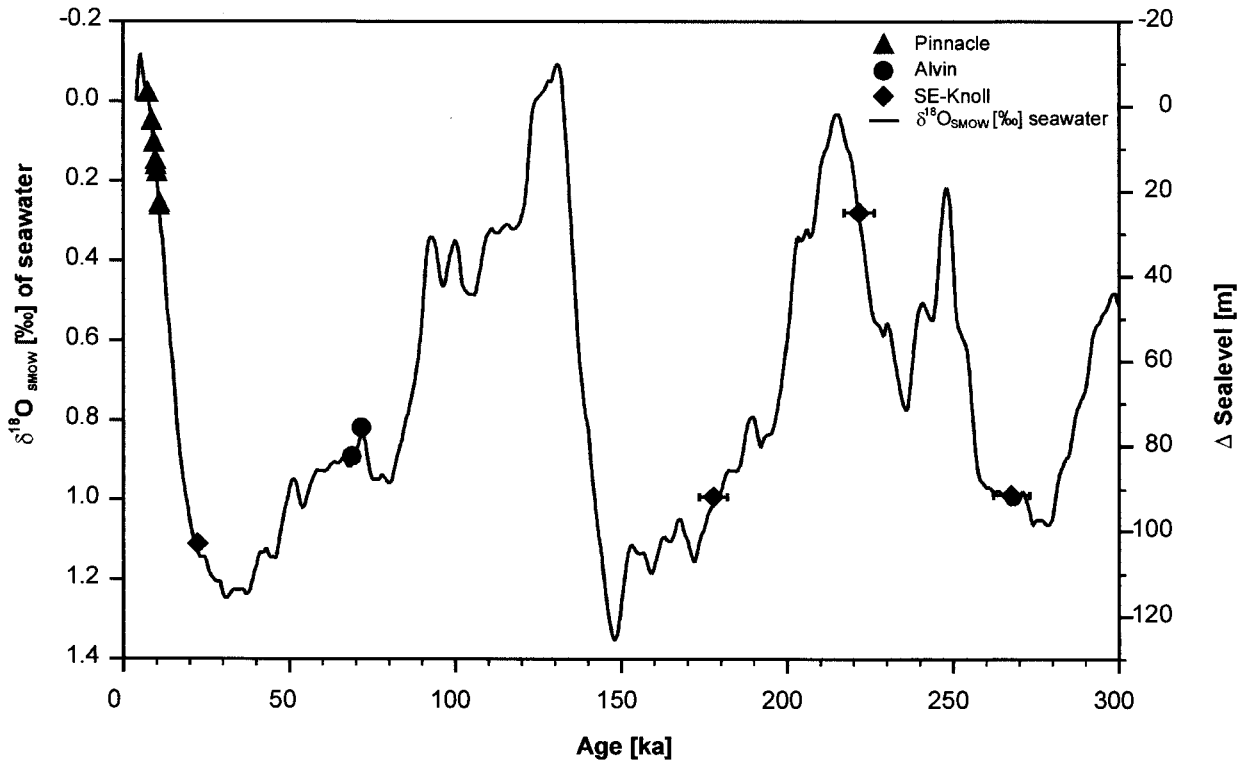


Fig. 5. Plot shows age as a function of the $\delta^{18}\text{O}_{\text{SMOW}}$ sealevel curve. On the secondary y-axis the Δ sealevel change is shown, assuming that the entire scale for the sealevel curve is about 1‰ (Schrug et al., 1996) and that the entire sealevel scale is 125 m (Fairbanks and Matthews, 1978; Fairbanks, 1989). The $\delta^{18}\text{O}_{\text{SMOW}}$ sealevel curve was obtained by assigning the first data point at 4 ka 0‰ SMOW (as the present seawater value) and multiplying with 1.03086 to account for the conversion from PDB to SMOW. Symbols show the $\delta^{18}\text{O}_{\text{SMOW}}$ for the seawater that the chemoherm carbonates precipitated from and the corresponding sealevel stand. Note that the age for 3429-3-A-8 is a mean value of sample a and b.

not necessarily apply for other isotopic stages (e.g., Labeyrie et al., 1987) but is a good approximation of the true value. The latter value of about 1‰ is in general accord with our findings that the $\delta^{18}\text{O}_{\text{PDB}}$ values of the chemoherm carbonates are up to about 0.9‰ heavier than predicted from modern seawater.

Past seawater temperatures during the time of the chemoherm precipitation (for details see Table 3) can be reconstructed using past $\delta^{18}\text{O}_{\text{SMOW}}$ seawater values (reconstructed from a recently published benthic stack from Karner et al., 2002) together with our $\delta^{18}\text{O}$ values from the chemoherm carbonates. Note, that seawater temperature reconstructions presented in Table 3 neglect any effect of pH, salinity and kinetic fractionation during gas hydrate formation.

From Table 3 and Figure 5 it can be seen that the reconstructed past seawater temperatures during carbonate precipitation vary in space and time between 2.6 and 8.6°C. The Holocene chemoherm samples from the Pinnacle indicate temperatures in between 2.6 and 4.2°C. In contrast, seawater temperatures reconstructed from the SE-Knoll and the Alvin chemoherm indicate temperatures during carbonate precipitation of between 3.7 to 8.6°C.

Temperature fluctuations in the order of about 1°C have already been observed in modern cold seeps fluids (Linke and Suess, 2001). However, our seawater temperature reconstruction indicates variations on the order of about 3°C. Temporal and spatial fluctuations of seawater temperature at cold seep

areas can be expected because of the glacial/interglacial changes of ocean currents and the temperature variations of seep fluids. At the moment, we can not make further refined inferences concerning seawater temperature changes. Further investigation may help to clarify if chemoherm carbonates can be used as a new archive for the reconstruction of past seawater temperature.

6. LATE QUATERNARY CHANGES OF FLUID FLOW IN THE HYDRATE RIDGE AREA

At Hydrate Ridge, advective fluid flow occurs mainly due to deformation-induced overpressuring of the sediment pore water. Overpressure can be produced by the following processes: (1) increase of compressive stress (i.e., reduction of the pore volume) caused by disequilibrium compaction and tectonic compression, (2) changes in the volume of the pore fluid caused by temperature increase (aquathermal pressuring), diagenesis and hydrocarbon generation, (3) fluid movement and (4) processes related to density differences between fluid and gas caused by a hydraulic (potentiometric) head, osmosis and buoyancy (Osborne and Swarbrick, 1997).

Many different processes can be postulated for the temporal modulation of the fluid flow causing short- and long-term variations. These include short-term variations in pressure associated with tides, ocean swell, storm surges, bottom current

velocities, biologic pumping, episodic gas release; long-term variations may result from tectonic processes, thermohaline convection, thermal convection and sealevel changes. For our observations at Hydrate Ridge, only the long-term variations of fluid flow are relevant. Tectonic processes are active on a time scale probably exceeding by far the observed variations and may therefore not be relevant. Fluid flow caused by haline convection can be excluded as driving mechanism for Hydrate Ridge from today's standard of knowledge. Likewise, changes in pore water volume due to temperature increase may also not be relevant for the cold seeps at Hydrate Ridge. There is only one instance of a warm pulse of advective fluid flow documented during long-term monitoring of ODP site 892 on Hydrate Ridge (Davis et al., 1995).

On the time scale of glacial/interglacial changes, their corresponding sealevel variations may significantly influence fluid flow at Hydrate Ridge. In particular, a glacial sealevel lowering would shift the bottom of the gas hydrate stability zone into shallower depths followed by gas hydrate decomposition in deeper sediments. Enhanced decomposition of gas hydrates may then generate enhanced gas and fluid flow in the cold seep areas. In addition, decomposition of gas hydrates as a consequence of the heightening of the gas hydrate stability zone also releases considerable amounts of fresh water into the sediment pore space thereby increasing pore fluid buoyancy. In this context, it is most crucial for fluid buoyancy that the hydraulic pressure of the ascending fluids in the plumbing system within the sediments has to exceed the pressure of the overlying seawater column (Carson and Screaton, 1998).

At least two scenarios can be distinguished when we consider pore water pressure changes due to sealevel variations: (1) seawater pressure exceeds the hydraulic pressure of the plumbing system below a chemoherm inhibiting the rise of fluids. (2) Seawater pressure is lower than the hydraulic pressure of the plumbing system and vigorous fluid venting occurs. Following this conceptual model, we propose that during glacial stages corresponding to low sealevel the pressure difference between water column and hydraulic pressure is largest. This triggers maximum rates of fluid flow through the chemoherm, extensive microbial activity and relatively large rates of carbonate precipitation. In contrast, the increase of the seawater pressure due to a climatically induced sealevel rise at glacial/interglacial transitions reduces the pressure difference between the ocean water column and the hydraulic pressure of the plumbing system. This effect restricted the flow rate and the corresponding rate of carbonate precipitation during interglacials. The latter scenario has already been observed for tidally controlled short-term sealevel fluctuations. High rates of fluid flow were measured at low tides whereas high tides were characterized by low rates of fluid flow (Linke et al., 1999; Tryon and Brown, 2001).

Besides sealevel oscillation there are other factors like density differences that are a possible explanation for fluid flow variations. The difference between the height of the water column and the height of the hydraulic head is crucial in controlling cold seep fluid flow. Thus, vigorous fluid flow may also be generated during sealevel highstands as long as the height of the hydraulic head exceeds the height of the water column. This interpretation may be valid for the Pinnacle samples showing U/Th ages corresponding to early Holocene ages from 7.3 to 11.4 ka when sealevel closely approached

present-day levels. These Holocene ages indicate that fluid venting started much later at this location than at the Alvin and SE-Knoll chemoherm.

Although a conceptual model for cold seep fluid flow is presented above, the relationship between climatically driven sealevel changes and enhanced carbonate precipitation at cold vent sites cannot be considered proven and must await further confirmation. In particular, factors not controlled by climate change like the fluid buoyancy or the height of the hydraulic head may cause fluid flow variations and have yet to be examined in detail in combination with hydrological and geophysical measurements. In addition, further U/Th measurements and drilling of chemoherm are required to better constrain the chronology of the geochemical evolution of the chemoherm carbonates relative to glacial/interglacial transitions during the Late Quaternary.

7. SUMMARY

U concentrations and $\delta^{234}\text{U}$ values are sensitive indicators for the fluid composition in cold seep sediments. Bottom water enriched in ^{234}U indicates a flux of U out of cold seep areas. It can be estimated that about 11% of the bottom water U originates from the sedimentary pore water. From the calculated pore water U flux (mean: $F_{\text{pw}} = 35 \pm 16 \text{ ng}/(\text{cm}^2 \cdot \text{a})$) and the reconstructed U pore water concentration (0.24 ng/g) a fluid flow between 46 cm/a and 353 cm/a (mean: $147 \pm 68 \text{ cm/a}$) can be estimated.

The U concentrations and $\delta^{234}\text{U}$ values of gas hydrate carbonates reflect their precipitation from bottom water and pore water under reducing conditions. Their U/Th ages reflect periods of intense fluid flow around 1.2 ± 0.3 and 4.7 ± 1.2 ka. Time intervals of enhanced carbonate precipitation may be controlled by earthquakes, vertical neotectonic movement and second order variations of the sealevel.

The chemoherm carbonates are precipitated mostly from bottom water and show U/Th ages from 7.3 up to 267.6 ka. Their U/Th ages tend to correspond to periods of low sealevel at glacial climatic stages. Presumably, the hydraulic pressure difference between the plumbing system below the chemoherm and the pressure of the water column control the outflow of hydrocarbon-rich fluids at the sediment-seawater interface.

The comparison of chemoherm $\delta^{18}\text{O}_{\text{PDB}}$ values with the marine $\delta^{18}\text{O}_{\text{SMOW}}$ record allows the reconstruction of seawater and/or fluid temperature during carbonate calcification. Seawater temperature variations from 2.6 to 8.6 °C reconstructed from the different chemoherm sites vary in space and time. Most likely, they reflect changes in ocean current temperature and/or fluid flow.

The correspondence of the chemoherm carbonate ages to glacial stages is interpreted to reflect sealevel variations. In a conceptual model, we infer that the hydraulic head is crucial for the rate of fluid flow. During glacials, when the pressure hydraulic head is low, extensive fluid flow occurs. In contrast, during interglacial periods, when the pressure of the hydraulic head is large, the rate of fluid flow is small.

Acknowledgments—This study was made possible by the programs TECFLUX I & II (Tectonically induced Fluxes, 03G0143A & 03G0148A) and LOTUS (Long-term Observatory for the Study of Control Mechanisms for the Formation and Destabilisation of Gas

Hydrates, 03G0165A) supported by the Bundesministerium für Bildung und Forschung (BMBF, Germany). This is publication GEOTECH-2 of the program GEOTECHNOLOGIEN of the BMBF and the Deutsche Forschungsgemeinschaft (DFG). Many thanks to F. Böhm and N. Gussone for helpful comments and discussions. Thanks to D. Rickert for providing Ca pore water concentrations. We thank the officers, crew and shipboard scientific parties of RV SONNE for excellent support during expeditions SO143 and SO148, especially the ROPOS crew. B. Domeyer, J. Heinze, A. Kolevica and R. Surberg are acknowledged for technical support. A Ph.D. scholarship to B.M.A. Teichert in the graduate school "Dynamik globaler Kreisläufe im System Erde" funded by the "Deutsche Forschungsgemeinschaft" (GRK 171) is gratefully acknowledged. The reviews of S.J.G. Galer, G.M. Henderson, J.M. Gieskes and S. Pichat helped significantly to improve this manuscript.

Associate editor: S. Galer

REFERENCES

- Aharon P. (1994) Geology and biology of modern and ancient submarine hydrocarbon seeps and vents: An introduction. *Geo-Marine Letters* **14**, 69–73.
- Aharon P., Roberts H. H., and Snelling R. (1992) Submarine venting of brines in the deep Gulf of Mexico: Observations and geochemistry. *Geology* **20**, 483–486.
- Aharon P., Schwarcz H. P., and Roberts H. H. (1997) Radiometric dating of submarine hydrocarbon seeps in the Gulf of Mexico. *Geol. Soc. Am. Bull.* **109**(5), 568–579.
- Barnes C. and Cochran J. K. (1988) The geochemistry of uranium in marine sediments. In *Radionuclides; a tool for oceanography* (eds. J. C. Guary, P. Guegueniat, and R. J. Pentreath), pp. 162–170. Elsevier.
- Barnes C. E. and Cochran J. K. (1990) Uranium removal in oceanic sediments and the oceanic U balance. *Earth Planet. Sci. Lett.* **97**, 94–101.
- Bassiot F. C., Labeyrie L. D., Vincent E., Quidelleur X., Shackleton N. J., and Lancelot Y. (1994) The astronomical theory of climate and the age of the Brunhes-Matuyama magnetic reversal. *Earth Planet. Sci. Lett.* **126**, 91–108.
- Boetius A., Ravenschlag K., Schubert C. J., Rickert D., Widdel F., Gieseke A., Amann R., Jorgensen B. B., Witte U., and Pfannkuche O. (2000) A marine microbial consortium apparently mediating anaerobic oxidation of methane. *Nature* **407**, 623–626.
- Böhm F., Joachimski M. M., Dullo W.-C., Eisenhauer A., Lehnert H., Reitner J., and Wörheide G. (2000) Oxygen isotope fractionation in marine aragonite of coralline sponges. *Geochim. Cosmochim. Acta* **64**(10), 1695–1703.
- Bohrmann G., Greinert J., Suess E., and Torres M. (1998) Authigenic carbonates from the Cascadia subduction zone and their relation to gas hydrate stability. *Geology* **26**(7), 647–650.
- Bohrmann G., Linke P., Suess E., and Pfannkuche O. (2000) *R/V SONNE cruise report, SO143 TECFLUX-I-1999*. GEOMAR, Kiel.
- Bohrmann G., Suess E., Greinert J., Teichert B. and Naehr T. (2002) Gas hydrate carbonates from Hydrate Ridge, Cascadia Convergent Margin: Indicators of near-seafloor clathrate deposits. *Proc. Fourth Int. Conf. Gas Hydrates*, pp. 102–107.
- Carson B. and Sreaton E. J. (1998) Fluid flow in accretionary prisms: Evidence for focused, time-variable discharge. *Rev. Geophys.* **36**(3), 329–351.
- Chen J. H., Edwards R. L., and Wasserburg G. J. (1986) ^{238}U , ^{234}U and ^{232}Th in seawater. *Earth Planet. Sci. Lett.* **80**, 241–251.
- Cheng H., Adkins J., Edwards R. L., and Boyle E. A. (2000a) U-Th dating of deep-sea corals. *Geochim. Cosmochim. Acta* **64**(14), 2401–2416.
- Cheng H., Edwards R. L., Hoff J., Gallup C. D., Richards D. A., and Asmerom Y. (2000b) The half-lives of uranium-234 and thorium-230. *Chem. Geol.* **169**, 17–33.
- Davis E. E., Becker K. Wang K. and Carson B. (1995) Long-term observations of pressure and temperature in Hole 892B, Cascadia accretionary prism. In *Cascadia Margin*, Proc. ODP, Sci. Res. 146, Pt.1. (ed. B. Carson, G. K. Westbrook, R. J. Musgrave, and E. Suess), pp. 299–311. College Station, TX (Ocean Drilling Program).
- Duncan R. A. and Kulm L. D. (1989) Plate tectonic evolution of the Cascades arc-subduction complex. In *The Eastern Pacific Ocean and Hawaii* (eds. E. L. Winterer, D. M. Hussong, and R. W. Decker), Vol. 1, pp. 413–438. Geological Society of America, Boulder, Colorado.
- Duplessy J.-C., Labeyrie L., and Waelbroeck C. (2002) Constraints on the ocean oxygen isotopic enrichment between the Last Glacial Maximum and the Holocene: Paleoceanographic implications. *Quat. Sci. Rev.* **21**, 315–330.
- Edwards R. L., Chen J. H., and Wasserburg G. J. (1987) ^{238}U - ^{234}U - ^{230}Th - ^{232}Th systematics and the precise measurement of time over the past 500,000 years. *Earth Planet. Sci. Lett.* **81**, 175–192.
- Edwards R. L., Beck J. W., Burr G. S., Donahue D. J., Chappell J. M. A., Bloom A. L., Druffel E. R. M., and Taylor F. W. (1993) A large drop in atmospheric $^{14}\text{C}/^{12}\text{C}$ and reduced melting in the Younger Dryas, documented with ^{230}Th ages of corals. *Science* **260**, 962–968.
- Eisenhauer A., Zhu Z. R., Collins L. B., Wyrwoll K. H., and Eichstatter R. (1996) The Last Interglacial sea level change: New evidence from the Abrolhos islands, West Australia. *Geol. Rundsch.* **85**, 606–614.
- Fairbanks R. G. (1989) A 17,000-year glacio-eustatic sea level record: Influence of glacial melting rates on the Younger Dryas event and deep-ocean circulation. *Nature* **342**, 637–642.
- Fairbanks R. G. and Matthews R. K. (1978) The marine oxygen isotope records in Pleistocene coral, Barbados, West Indies. *Quat. Res.* **10**, 181–196.
- Ferrel R. E. and Aharon P. (1994) Mineral assemblages occurring around hydrocarbon vents in the northern Gulf of Mexico. *Geo-Marine Letters* **14**, 74–80.
- Friedman I., and O'Neil J. R. (1977) Compilation of stable isotope fractionation factors of geochemical interest. *U. S. Geol. Surv. Prof. Pap.* 440-KK. U.S. Geological Survey, Reston, VA.
- Goldfinger C., Kulm L. D., Yeats R. S., McNeill L., and Hummon C. (1997) Oblique strike-slip faulting of the central Cascadia submarine forearc. *J. Geophys. Res.* **102**(B4), 8217–8243.
- Greinert J., Bohrmann G., and Suess E. (2001) Gas hydrate-associated carbonates and methane-venting at Hydrate Ridge: Classification, distribution and origin of authigenic lithologies. In *Natural gas hydrates: Occurrence, distribution, and detection* (eds. C. K. Paull and W. P. Dillon), Vol. 124, pp. 99–113. American Geophysical Union, Washington, DC.
- Henderson G. M., Slowey N. C., and Haddad G. A. (1999) Fluid flow through carbonate platforms: Constraints from $^{234}\text{U}/^{238}\text{U}$ and Cl⁻ in Bahamas pore-waters. *Earth Planet. Sci. Lett.* **169**, 99–111.
- Herzig P., Suess E., and Linke P. (1997) *R/V SONNE cruise report, SO109: Hydrotrace*. GEOMAR, Kiel.
- Holbrook W. S., Hoskins H., Wood W. T., Stephen R. A., Lizzaralde D., and Party L. S. (1996) Methane hydrate and free gas on the Blake Ridge from vertical seismic profiling. *Science* **273**, 1840–1843.
- Hudson T. L. and Magoon L. B. (2002) Tectonic control on greenhouse gas flux to the Paleogene atmosphere from the Gulf of Alaska accretionary prism. *Geology* **30**(6), 547–550.
- Ivanovich M. and Harmon R. S. (1992) *Uranium-series disequilibrium: Applications to earth, marine, and environmental sciences*. (2nd edition). Oxford University Press, Oxford.
- Jaffey A. H., Flynn K. F., Glendenin L. E., Bentley W. C., and Essling A. M. (1971) Precision measurements of half-lives and specific activities of ^{235}U and ^{238}U . *Phys. Rev. Lett.* **4**, 1889–1906.
- Karner D. B., Levine J., Medeiros B. P., and Muller R. A. (2002) Constructing a stacked benthic $\delta^{18}\text{O}$ record. *Paleoceanography* **17**(3), 10.1029/2001PA000667.
- Kigoshi K. (1971) Alpha-recoil thorium-234; dissolution into water and the uranium-234/uranium-238 disequilibrium in nature. *Science* **173**, 47–48.
- Kulm L. D., Suess E., Moore J. C., Carson B., Lewis B. T., Ritger S. D., Kadko D. C., Thornburg T. M., Embley R. W., Rugh W. D., Massoth G. J., Langseth M. G., Cochrane G. R., and Scamman R. L. (1986) Oregon subduction zone: Venting, fauna, and carbonates. *Science* **231**, 561–566.
- Labeyrie L. D., Duplessy J. C., and Blanc P. L. (1987) Variations in mode of formation and temperature of oceanic deep waters over the past 125 000 years. *Nature* **327**, 477–482.
- Linke P. and Suess E. (2001) *R/V SONNE cruise report, SO148 TECFLUX-II-2000*. GEOMAR, Kiel.

- Linke P., Pfannkuche O., Torres M. E., Collier R. W., Witte U., McManus J., Hammond D. E., Brown K. M., Tryon M. D., and Nakamura K. (1999) Variability of benthic flux and discharge rates at vent sites determined by in situ instruments. *EOS Transactions AGU*. **80**(46), F509.
- Ludwig K. R. and Titterton D. M. (1994) Calculation of $^{230}\text{Th}/\text{U}$ isochrons, ages, and errors. *Geochim. Cosmochim. Acta* **58**(22), 5031–5042.
- Moore J. C., Orange D., and Kulm L. D. (1990) Interrelationship of fluid venting and structural evolution: Alvin observations from the frontal accretionary prism, Oregon. *J. Geophys. Res.* **95**(B6), 8795–8808.
- Nikolayev D. S., Lazarev K. F., Korn O. P., and Drozhzhin V. M. (1966) Geochemical balance of radioactive elements in the basin of the Black Sea. *Radiokhim.* **8**, 469–476.
- Osborne M. J. and Swarbrick R. E. (1997) Mechanisms for generating overpressure in sedimentary basins: A reevaluation. *AAPG Bull.* **81**(6), 1023–1041.
- Pirazzoli P. A. (1991) *World Atlas of Holocene Sea-Level Changes*. Elsevier.
- Polikarpov G. G., Egorov V. N., Gulin S. B., Gulin M. B., and Stokozov N. A. (1992) Gas seeps from the bottom of the Black Sea - a new object of molismology. In *Molismology of the Black Sea* (ed. G. G. Polikarpov), pp. 10–28, Naukova Dumka, Kiev (in Russian).
- Rendsbergen P. V., Batist M. D., Klerkx J., Hus R., Poort J., Vanneste M., Granin N., Khlystov O., and Krinitsky P. (2002) Sublacustrine mud volcanoes and methane seeps caused by dissociation of gas hydrates in Lake Baikal. *Geology* **30**(7), 631–634.
- Schrag D. P., Hampt G., and Murray D. W. (1996) Pore fluid constraints on the temperature and oxygen isotope composition of the glacial ocean. *Science* **272**, 1930–1932.
- Shen G. T. and Dunbar R. B. (1995) Environmental controls on uranium in reef corals. *Geochim. Cosmochim. Acta* **59**(10), 2009–2024.
- Sibuet M. and Olu K. (1998) Biogeography, biodiversity and fluid dependence of deep-sea cold-seep communities at active and passive margins. *Deep-Sea Res. II* **45**, 517–567.
- Sloan L. C., Walker J. C. G., Moore T. C. Jr., Rea D. K., and Zachos J. C. (1992) Possible methane-induced polar warming in the early Eocene. *Nature* **357**, 320–322.
- Suess E., Torres M. E., Bohrmann G., Collier R. W., Greinert J., Linke P., Rehder G., Tréhu A., Wallmann K., Winckler G., and Zuleger E. (1999) Gas hydrate destabilization: Enhanced dewatering, benthic material turnover and large methane plumes at the Cascadia convergent margin. *Earth Planet. Sci. Lett.* **170**, 1–15.
- Suess E., Torres M. E., Bohrmann G., Collier R. W., Rickert D., Goldfinger C., Linke P., Heuser A., Sahling H., Heeschen K., Jung C., Nakamura K., Greinert J., Pfannkuche O., Tréhu A., Klinkhammer G., Whiticar M. J., Eisenhauer A., Teichert B., and Elvert M. (2001) Sea floor methane hydrates at Hydrate Ridge, Cascadia Margin. In *Natural Gas Hydrates: Occurrence, Distribution, and Dynamics* (eds. C. K. Paull and W. P. Dillon), Vol. 124, pp. 87–98. American Geophysical Union, Washington, DC.
- Torres M. E., Bohrmann G., Brown K., deAngelis M., Hammond D., Klinkhammer G., McManus J., Suess E., Tréhu A. (1999) *Geochemical observations on Hydrate Ridge, Cascadia Margin during R/V-ATLANTIS-Cruise AT3-35b, July 1999*. Oregon State University.
- Torres M. E., McManus J., Hammond D. E., Angelis M. A. d., Heeschen K. U., Colbert S. L., Tryon M. D., Brown K. M., and Suess E. (2002) Fluid and chemical fluxes in and out of sediments hosting methane hydrate deposits on Hydrate Ridge, OR, I: Hydrological provinces. *Earth Planet. Sci. Lett.* **201**(3–4), 525–540.
- Tréhu A. M., Torres M. E., Moore G. F., Suess E., and Bohrmann G. (1999) Temporal and spatial evolution of a gas hydrate-bearing accretionary ridge on the Oregon continental margin. *Geology* **27**(10), 939–942.
- Tryon M. D. and Brown K. M. (2001) Complex flow patterns through Hydrate Ridge and their impact on seep biota. *Geophys. Res. Lett.* **28**(14), 2863–2866.
- Wachter E. and Hayes J. M. (1985) Exchange of oxygen isotopes in carbon-dioxide - phosphoric acid systems. *Chem. Geology* **52**, 365–374.
- Westbrook G. K., Carson B., Musgrave R. J., and et al. (1994) *Proc. ODP, Init. Repts.*, 146, Pt.1. College Station, TX. (Ocean Drilling Program).

APPENDIX 1

Binary mixing calculation in order to estimate U_{pw} Calculation of mixing factor X:

$$\delta^{234}U_{bw} = X \cdot \delta^{234}U_{pw} + (1 - X) \cdot \delta^{234}U_{sw}$$

It follows:

$$X = (\delta^{234}U_{bw} - \delta^{234}U_{sw}) / (\delta^{234}U_{pw} - \delta^{234}U_{sw})$$

Calculation of U_{pw} :

$$U_{pw} = (U_{bw} - (1 - X) \cdot U_{sw}) / X$$

APPENDIX 2

Estimation of the F_{pw} using a 1-box-model

$$\delta^{234}U_{bw} \cdot F_{bw} = \delta^{234}U_{sw} \cdot F_{sw} + \delta^{234}U_{pw} \cdot F_{pw}$$

with:

$$F_{bw} = F_{sw} + F_{pw}$$

It follows:

$$F_{pw} = F_{sw} \cdot ((\delta^{234}U_{bw} - \delta^{234}U_{sw}) / (\delta^{234}U_{pw} - \delta^{234}U_{sw}))$$